An experimental and kinetic modeling study of premixed NH3/CH4/O2/Ar flames at low pressure

ARTICLE *in* COMBUSTION AND FLAME · MARCH 2013

Impact Factor: 3.08 · DOI: 10.1016/j.combustflame.2009.03.005

5 AUTHORS, INCLUDING:

Zhen-Yu Tian
Chinese Academy of Sciences
66 PUBLICATIONS **884** CITATIONS
SEE PROFILE

P. Glarborg
Technical University of Denmark
196 PUBLICATIONS **5,651** CITATIONS
SEE PROFILE

Combustion and Flame 156 (2009) 1413–1426

Contents lists available at ScienceDirect

Combustion and Flame

journal homepage: www.elsevier.com/locate/combustflame

An experimental and kinetic modeling study of premixed $NH_3/CH_4/O_2/Ar$ flames at low pressure

Zhenyu Tian [a], Yuyang Li [a], Lidong Zhang [a], Peter Glarborg [b,*], Fei Qi [a,*]

[a] National Synchrotron Radiation Laboratory, University of Science and Technology of China, Hefei, Anhui 230029, PR China
[b] Department of Chemical and Biochemical Engineering, Technical University of Denmark, DK-2800 Lyngby, Denmark

ARTICLE INFO

Article history:
Received 2 October 2008
Received in revised form 6 January 2009
Accepted 4 March 2009
Available online 6 May 2009

Keywords:
$NH_3/CH_4/O_2/Ar$ flame
Kinetic modeling
Molecular-beam mass spectrometry
Tunable synchrotron VUV photoionization

ABSTRACT

An experimental and modeling study of 11 premixed $NH_3/CH_4/O_2/Ar$ flames at low pressure (4.0 kPa) with the same equivalence ratio of 1.0 is reported. Combustion intermediates and products are identified using tunable synchrotron vacuum ultraviolet (VUV) photoionization and molecular-beam mass spectrometry. Mole fraction profiles of the flame species including reactants, intermediates and products are determined by scanning burner position at some selected photon energies near ionization thresholds. Temperature profiles are measured by a Pt/Pt–13%Rh thermocouple. A comprehensive kinetic mechanism has been proposed. On the basis of the new observations, some intermediates are introduced. The flames with different mole ratios (R) of NH_3/CH_4 (R0.0, R0.1, R0.5, R0.9 and R1.0) are modeled using an updated detailed reaction mechanism for oxidation of CH_4/NH_3 mixtures. With R increasing, the reaction zone is widened, and the mole fractions of H_2O, NO and N_2 increase while those of H_2, CO, CO_2 and NO_2 have reverse tendencies. The structural features by the modeling results are in good agreement with experimental measurements. Sensitivity and flow rate analyses have been performed to determine the main reaction pathways of CH_4 and NH_3 oxidation and their mutual interaction.

1. Introduction

Since ammonia is present in higher concentration than other fuel-nitrogen species in volatiles from biomass feedstocks [1] and the NO_x emission from combustion of biomass and other solid fuels is of great interest, numerous experimental and modeling studies of the NH_3-doped flames were reported previously [2–13]. Puechberty and Cottereau [2] performed an experimental investigation of NO formation in a low-pressure NH_3-doped CH_4/O_2 flame with mass spectrometry and absorption spectroscopy. They reported concentration profiles of major species, i.e. CH_4, H_2, CO_2, O_2 and H_2O, together with OH and nitrogenous species such as NH_2, NH, CN, NH_3, NO and NO_2 [2]. Rosier et al. [3] measured CO and H_2O concentration profiles with tunable diode laser spectroscopy under the same condition as that of Puechberty and Cottereau. Bian et al. [4,5] reported HNO concentration and Garo et al. [6] reported concentration profiles of some major species, stable intermediates (HCN) and radicals (H, O, OH and CH_3) in NH_3-doped CH_4/O_2 flames with mass spectrometry, absorption spectroscopy and laser-induced fluorescence. Later, Williams and Fleming [7] measured the relative concentration profiles of CN, NH, NCO, NH_2 and NO in a low-pressure NH_3-doped $CH_4/O_2/Ar$ flame. In 2002, Sullivan et al. [8] investigated NH_3 conversion in laminar, NH_3-seeded N_2-diluted CH_4 diffusion flames and concluded that as more NH_3 was added, a greater percentage was converted to N_2 rather than NO. After that, Rahinov et al. [9] measured the NH_2 absolute concentration profiles by intracavity laser absorption spectroscopy in CH_4/air laminar flames doped with trace amounts of NH_3 at the pressure of 4.0 kPa. Moreover, Dyakov et al. [10] reported the sampling measurements of NO in $CH_4/O_2/CO_2$ doped with NH_3. Besides these experimental studies, there are some theoretical investigations focusing on the formation and consumption pathways of NO_x in NH_3-doped flames [11–13]. Reactions HNO + H = NO + H_2, NO + H = N + OH, NO + N = N_2 + O and NH + NO = N_2 + OH were reported as the key reactions contributing to NO production and consumption [12]. More recently, Skreiberg et al. [14] developed a chemical kinetic model for oxidation of NH_3 in the presence and absence of CH_4 [14]. The kinetic model was validated against flow-reactor experiments over a wide range of condition. Skreiberg et al. [14] concluded that NO is partly converted to HCN by reaction with CH_3 in the presence of CH_4, but did not include a full subset for hydrocarbon/amine interactions [14].

The previous flame studies have provided important information on the structure of $NH_3/CH_4/O_2$ flames, but identification of combustion species, especially intermediates, and the effect of mole ratio (R) of NH_3/CH_4 on mole fractions of flame species in $NH_3/CH_4/O_2$ flames are lacking. The objective of the current work is to identify a more complete set of flame species and to illustrate the effect of R on concentrations of major species

* Corresponding authors. Fax: +86 551 5141078.
E-mail addresses: PGL@kt.dtu.dk (P. Glarborg), fqi@ustc.edu.cn (F. Qi).

0010-2180/$ - see front matter © 2009 The Combustion Institute. Published by Elsevier Inc. All rights reserved.
doi:10.1016/j.combustflame.2009.03.005

and some intermediates with the molecular-beam mass spectrometry (MBMS) and tunable synchrotron VUV photoionization. The high energy resolution and wide energy range of synchrotron VUV light can help distinguish most isomers, and reduce fragmentation via near-threshold photoionization, leading to the unambiguous detection of radicals. For example, this method can identify radicals and isomers (e.g., enols and aldehydes) in hydrocarbon flames [15–17]. Moreover, the data from the flames *R*0.0, *R*0.1, *R*0.5, *R*0.9 and *R*1.0 are compared with modeling predictions using an updated chemical kinetic model, based on the work of Skreiberg et al. [14]. The detailed flame composition profiles provide a demanding test of the kinetic model and the data are helpful in extending the knowledge of ammonia chemistry.

2. Experimental methods

The experiments were performed at the National Synchrotron Radiation Laboratory (NSRL), Hefei, China. The experimental setup has been described previously [18], and a newly constructed beamline from undulator radiation was used for this study. A 1 m Seya–Namioka monochromator was used to disperse synchrotron radiation from an undulator beamline of the 800 MeV electron storage ring. The energy resolving power $E/\Delta E$ (FWHM) is about 1000 with the average photon flux of about 10^{13} photons/s. A gas filter with inert gas (Ne or Ar) was used to eliminate higher-order harmonic radiation. The photon flux was monitored by a silicon photodiode (SXUV-100) to normalize ion signals.

A movable McKenna burner with 6 cm in diameter is mounted in the flame chamber. Flame species are sampled by a cone-shaped quartz nozzle with a 40° included angle and a ~500 μm orifice at the tip. The sampled gas forms a molecular beam which then passes into a differentially pumped ionization region through a nickel skimmer. The molecular beam is crossed with the tunable VUV light in the photoionization chamber and the photoions are collected and analyzed by a reflectron time-of-flight mass spectrometer (RTOF-MS) with an approximate mass resolution of 1400 [19] and a detection limit of about 1 part per million (ppm). Then the ion signals are amplified by a pre-amplifier (VT120C, ORTEC, USA) and recorded using a multiscaler (FAST Comtec P7888, Germany) with a bin width of 2 ns. A digital delay generator (DG535, USA) is used to trigger a pulsed power supply and the multiscaler as well. Eleven flames with the same equivalence ratio of 1.0 but different *R* varying from 0.0 to 1.0 were studied, as shown in Table 1. The flow rate of Ar had a constant value of 1.000 standard liter per minute (SLM) for all flames. Flow rates of CH_4, NH_3, O_2 and Ar were separately controlled by MKS mass flow controllers. The flame was stabilized on the burner at a pressure of 4.0 kPa, with inlet cold-flow velocity of 41 cm/s at 300 K. The equivalence ratio is calculated considering the following oxidation reaction,

$$x\mathrm{CH_4} + y\mathrm{NH_3} + (2x + 1.25y)\mathrm{O_2} \rightarrow x\mathrm{CO_2} + y\mathrm{NO} + (2x + 1.5y)\mathrm{H_2O}. \quad (1)$$

NO is considered as the final NO_x product since it is more stable than NO_2 at high temperature [20].

The temperature profiles of the investigated flames were measured with a Pt/Pt–13%Rh thermocouple, 0.076 mm in diameter, coated with Y_2O_3–BeO anti-catalytic ceramic. The position of the butt-welded junction was located at 20 mm upstream from the quartz nozzle. The thermal disturbances are resulted from heat transfer between the thermocouple and its surroundings. Conduction losses are negligible if the wire length is 160 times larger than its diameter [21,22]. The length of the thermocouple used in this work is about 78 mm, which is about 1000 times of its diameter. In this work, measured temperature profiles are calibrated for modeling work, considering radiation heat losses given by the following equation [23]:

$$T_c - T_m = \frac{\varepsilon\sigma d(T_m^4 - T_w^4)}{2\lambda}, \quad (2)$$

where T_c, T_m and T_w are calibrated, measured and wall temperatures, respectively; ε is the emissivity of the Y_2O_3–BeO coating; σ is the Stefan–Boltzmann constant; d is the diameter of the thermocouple and λ is the gas thermal conductivity. Fristrom [23] concluded that T_c was about 100 K higher than T_m at an upper limit. In previous MBMS investigation of a low-pressure ethane flame, a decrease of the measured flame temperature by 100 K was adopted to account for the cooling effect of the probe [24]. Based on the reproducibility of the measurement, the temperature errors are estimated to be ±100 K, within which the modeling results with T_c have a 3% uncertainty for the major species and about 10% for intermediates in the flame *R*1.0, as seen in Figs. S1–S3 in Supplemental material.

With the variation of photon energy, a series of mass spectra were measured in the middle of the luminous region. The integrated ion intensities for a specified mass are normalized by the photon flux, and then plotted as a function of the photon energy, yielding photoionization efficiency (PIE) spectrum which contains precise information of ionization energies (IEs) of the specific species. Kamphus et al. [25] measured the cooling effect of the quartz nozzle and found final rotational temperatures of 300–400 K. The molecular-beam rotational temperature was independent of the initial temperature. Considering the cooling effect of molecular beam, the experimental errors for determining IEs in this study are within 0.05 eV for stable species and slightly higher for some radicals because of the weak signal-to-noise ratio.

The detailed evaluation method of mole fraction has been described previously [26]. To avoid fragmentation of intermediates and differentiate N_2 and CO, mass spectra for calculating mole fractions are recorded at the following energies: 16.53, 14.59, 12.92, 11.81 and 10.00 eV. The uncertainties of the mole fractions are ±5–10% for the major species, ±25% for intermediates with known photoionization cross sections (C_2H_2 and C_2H_4) and a factor of two

Table 1
Flame conditions of the $NH_3/CH_4/O_2$/Ar flames.

R[a]	Flow rate[b] (SLM)			D_M[c] (g/s/cm^2)
	CH_4	O_2	NH_3	
0.0	0.500	1.000	0.000	1.928E−3
0.1	0.465	0.989	0.047	1.926E−3
0.2	0.435	0.978	0.087	1.922E−3
0.3	0.408	0.970	0.122	1.920E−3
0.4	0.385	0.961	0.154	1.917E−3
0.5	0.364	0.954	0.182	1.915E−3
0.6	0.345	0.948	0.207	1.913E−3
0.7	0.328	0.942	0.230	1.912E−3
0.8	0.313	0.937	0.250	1.910E−3
0.9	0.299	0.932	0.269	1.909E−3
1.0	0.286	0.928	0.286	1.907E−3

[a] *R* refers to the mole ratio of NH_3/CH_4.
[b] Flow rate of Ar is 1.000 SLM for all the 11 flames.
[c] D_M is the mass flow rate of the gas mixture.

Table 2
Selected reactions in the hydrocarbon and amine subsets. Units are cm, mol, s, cal.

	Selected reactions	A	n	E_a	Ref.
CH_i subset					
1.	$CH_2 + H(+M) = CH_3(+M)$	3.8E16	−0.80	0	[82]
	Low-pressure limit	4.8E27	−3.14	1230	
	Troe parameters: 0.468 78 1995 5590				
	Third body efficiencies: $N_2 = 1.3$, $H_2O = 6$, Ar = 0.7				
2.	$CH_3 + H = CH_2 + H_2$	9.0E13	0.00	15,100	[20]
3.	$CH_2 + H_2 = CH_3 + H$	7.2E13	0.00	0	[20]
4.	$CH_3 + O = CH_2O + H$	6.9E13	0.00	0	[30]
5.	$CH_3 + O = CO + H_2 + H$	1.5E13	0.00	0	[30]
6.	$CH_3 + OH = {}^3CH_2 + H_2O$	1.1E03	3.00	2780	[83]
7.	$CH_3 + OH = {}^1CH_2 + H_2O$	4.4E13	−0.3485	−727	[39] 0.04 atm fit
8.	$CH_3 + HO_2 = CH_3O + OH$	2.0E13	0.00	1075	[30]
9.	$CH_3 + O_2 = CH_3O + O$	7.5E12	0.00	28,297	[30]
10.	$CH_3 + O_2 = CH_2O + OH$	1.9E11	0.00	9842	[30]
11.	$CH_2 + M = CH + H + M$	5.6E15	0.00	89,000	[84]
12.	$CH_2 + M = C + H_2 + M$	5.8E12	0.00	68,500	[84]
13.	$CH_2 + H = CH + H_2$	1.2E14	0.00	0	[44]
14.	$CH_2 + O = CO + H + H$	1.2E14	0.00	536	[44]
15.	$CH_2 + O = CO + H_2$	8.0E13	0.00	536	[44]
16.	$CH_2 + OH = CH_2O + H$	2.8E13	0.1228	−161	[85]
17.	$CH_2 + OH = CH + H_2O$	8.6E05	2.019	6776	[85]
18.	$CH_2 + O_2 = CO + H_2O$	1.8E11	0.00	0	[44] est 10%
19.	$CH_2 + O_2 = CO_2 + H + H$	3.8E11	0.00	0	[44,86]
20.	$CH_2 + O_2 = CO_2 + H_{2t}$	3.4E11	0.00	0	[44,86]
21.	$CH_2 + O_2 = CO + OH + H$	6.1E11	0.00	0	[44,86]
22.	$CH_2 + CO_2 = CO + CH_2O$	1.0E11	0.00	1000	[20]
23.	$^1CH_2 + M = CH_2 + M$	1.0E13	0.00	0	[20]
	Third body efficiencies: $N_2 = 0$, Ar = 0, H = 20				
	$^1CH_2 + N_2 = CH_2 + N_2$	1.3E13	0.00	430	[20]
	$^1CH_2 + Ar = CH_2 + Ar$	1.5E13	0.00	884	[20]
24.	$^1CH_2 + H = CH + H_2$	3.0E13	0.00	0	[20]
25.	$^1CH_2 + O = CO + H + H$	3.0E13	0.00	0	[20]
26.	$^1CH_2 + OH = CH_2O + H$	3.0E13	0.00	0	[20]
27.	$^1CH_2 + O_2 = CH_2 + O_2$	3.1E13	0.00	0	[44]
28.	$^1CH_2 + H_2O = CH_2O + H_2O$	3.0E13	0.00	0	[20]
29.	$^1CH_2 + CO_2 = CH_2O + CO$	1.1E13	0.00	0	[87]
30.	$CH + H = C + H$	1.5E14	0.00	0	[20]
31.	$CH + O = CO + H$	5.7E13	0.00	0	[20]
32.	$CH + OH = HCO + H$	3.0E13	0.00	0	[20]
33.	$CH + OH = C + H_2O$	4.0E07	2.00	0	[20]
34.	$CH + O_2 = HCO + O$	3.3E13	0.00	0	[20]
35.	$CH + H_2O = CH_2O + H$	5.7E12	0.00	−755	[20]
36.	$CH + CO_2 = HCO + CO$	8.8E06	1.75	−1040	[87]
37.	$C + OH = CO + H$	5.0E13	0.00	0	[20]
38.	$C + O_2 = CO + O$	2.0E13	0.00	0	[20]
NH_i subset (selected reactions)					
39.	$NH_2 + O = HNO + H$	6.6E13	0.00	0	See text
40.	$NH_2 + O = NH + OH$	7.0E12	0.00	0	See text
	$NH_2 + O = NH + OH$ Duplicate reaction	8.6E−1	4.01	1673	[48]
41.	$N + NO = N_2 + O$	2.1E13	0.00	0	[44]
CH_i/NH_j subset (selected reactions)					
42.	$CH_4 + NH_2 = CH_3 + NH_3$	1.5E03	3.01	9940	[88]
43.	$CH_3 + NH_2 = CH_3NH_2$	1.3E54	−12.72	15,608	[54] 0.1 atm
44.	$CH_3 + NH_2 = CH_2NH_2 + H$	1.1E13	−0.13	9905	[54] 0.1 atm
45.	$CH_3 + NH_2 = CH_3NH + H$	1.2E13	−0.15	16,144	[54] 0.1 atm
46.	$CH_3 + NH_2 = CH_2NH + H_2$	2.1E11	−0.10	19,095	[54] 0.1 atm
47.	$CH_3 + NH_2 = CH_4 + NH$	2.8E06	1.94	9210	[54]
48.	$CH_3 + NH_2 = CH_2 + NH_3$	1.6E06	1.87	7570	[54]
49.	$CH_3 + NH = CH_2NH + H$	4.0E13	0.00	0	[54]
50.	$CH_3 + NH = CH_4 + N$	8.2E05	1.87	5852	[54]
51.	$CH_3 + N = H_2CN + H$	7.1E13	0.00	0	[20]
52.	$^1CH_2 + NH_3 = CH_2NH + H + H$	1.0E14	0.00	0	Est
53.	$^1CH_2 + NH_2 = CH_2NH + H$	3.0E13	0.00	0	Est
54.	$CH + NH_3 = H_2CN + H + H$	4.4E13	0.00	−630	[89]
55.	$CH + NH_2 = H_2CN + H$	3.0E13	0.00	0	Est
56.	$CH + NH = HCN + H$	3.0E13	0.00	0	Est
57.	$CH + N = CN + H$	1.3E13	0.00	0	[20]
58.	$CH_3NH_2 + M = CH_2NH + H_2$	2.4E13	0.00	107,260	[90]
59.	$CH_3NH_2 + H = CH_2NH_2 + H_2$	5.6E08	1.50	5464	[54]
60.	$CH_3NH_2 + H = CH_3NH + H_2$	4.8E08	1.50	9706	[54]
61.	$CH_3NH_2 + O = CH_2NH_2 + OH$	4.0E08	1.50	5196	[54]
62.	$CH_3NH_2 + O = CH_3NH + OH$	3.3E08	1.50	6348	[54]
63.	$CH_3NH_2 + OH = CH_2NH_2 + H_2O$	1.0E13	0.00	0	[91]
64.	$CH_3NH_2 + OH = CH_3NH + H_2O$	2.4E06	2.00	447	[54]
65.	$CH_3NH_2 + CH_3 = CH_2NH_2 + CH_4$	1.5E06	1.87	9170	[54]
66.	$CH_3NH_2 + CH_3 = CH_3NH + CH_4$	1.6E06	1.87	8842	[54]
67.	$CH_3NH_2 + NH_2 = CH_2NH_2 + NH_3$	2.8E06	1.94	5494	[54]
68.	$CH_3NH_2 + NH_2 = CH_3NH + NH_3$	1.8E06	1.94	7143	[54]
69.	$CH_2NH_2 = CH_2NH + H$	1.1E45	−10.24	47,817	[54] 0.1 atm
70.	$CH_2NH_2 + H = CH_2NH + H_2$	4.8E08	1.50	−894	[54]
71.	$CH_2NH_2 + O = CH_2O + NH_2$	7.0E13	0.00	0	[54]
72.	$CH_2NH_2 + O = CH_2NH + OH$	3.3E08	1.50	−894	[54]
73.	$CH_2NH_2 + OH = CH_2OH + NH_2$	4.0E13	0.00	0	[54]
74.	$CH_2NH_2 + OH = CH_2NH + H_2O$	2.4E06	2.00	−1192	[54]
75.	$CH_2NH_2 + O_2 = CH_2NH + HO_2$	1.0E22	−3.09	6756	[54]
76.	$CH_2NH_2 + CH_3 = C_2H_5 + NH_2$	2.0E13	0.00	2702	[54]
77.	$CH_2NH_2 + CH_3 = CH_2NH + CH_4$	1.6E06	1.87	−626	[54]
78.	$CH_3NH = CH_2NH + H$	1.6E36	−7.92	36,342	[54] 0.1 atm
79.	$CH_3NH + H = CH_2NH + H_2$	7.2E08	1.50	−894	[54]
80.	$CH_3NH + O = CH_2NH + OH$	5.0E08	1.50	−894	[54]
81.	$CH_3NH + OH = CH_2NH + H_2O$	3.6E06	2.00	−1192	[54]
82.	$CH_3NH + CH_3 = CH_2NH + CH_4$	2.4E06	1.87	−1113	[54]
83.	$CH_2NH + H = H_2CN + H_2$	2.4E08	1.50	7322	[54]
84.	$CH_2NH + H = HCNH + H_2$	3.0E08	1.50	6130	[54]
85.	$CH_2NH + O = H_2CN + OH$	1.7E08	1.50	4630	[54]
86.	$CH_2NH + O = HCNH + OH$	2.2E08	1.50	5404	[54]
87.	$CH_2NH + O = CH_2O + NH$	1.7E06	2.08	0	[54]
88.	$CH_2NH + OH = H_2CN + H_2O$	1.2E06	2.00	−89	[54]
89.	$CH_2NH + OH = HCNH + H_2O$	2.4E06	2.00	457	[54]
90.	$CH_2NH + CH_3 = H_2CN + CH_4$	8.2E05	1.87	7123	[54]
91.	$CH_2NH + CH_3 = HCNH + CH_4$	5.3E05	1.87	9687	[54]
92.	$CH_2NH + NH_2 = H_2CN + NH_3$	9.2E05	1.94	4441	[54]
93.	$CH_2NH + NH_2 = HCNH + NH_3$	1.8E06	1.94	6090	[54]
94.	$H_2CN = HCN + H$	1.3E29	−6.03	29,894	[54] 0.1 atm
95.	$H_2CN + H = HCN + H_2$	2.4E08	1.50	−894	[54]
96.	$H_2CN + O = HCN + OH$	1.7E08	1.50	−894	[54]
97.	$H_2CN + OH = HCN + H_2O$	2.1E17	−1.68	318	[54] 0.1 atm
	$H_2CN + OH = HCN + H_2O$	1.2E06	2.00	−1192	Duplicate reaction
98.	$H_2CN + O_2 = CH_2O + NO$	3.0E12	0.00	5961	[54]
99.	$H_2CN + NH_2 = HCN + NH_3$	9.2E05	1.94	−1152	[54]
100.	$H_2CN + NH = HCN + NH_2$	1.7E08	1.50	−894	Est k_{95}
101.	$H_2CN + N = CH_2 + N_2$	2.0E13	0.00	0	[20]
102.	$HCNH = HCN + H$	7.7E25	−5.20	21,986	[54] 0.1 atm
103.	$HCNH + H = H_2CN + H$	2.0E13	0.00	0	[54]
104.	$HCNH + H = HCN + H_2$	2.4E08	1.50	−894	[54]
105.	$HCNH + O = HNCO + H$	7.0E13	0.00	0	[54]
106.	$HCNH + O = HCN + OH$	1.7E08	1.50	−894	[54]
107.	$HCNH + OH = HCN + H_2O$	1.2E06	2.00	−1192	[54]
108.	$HCNH + CH_3 = HCN + CH_4$	8.2E05	1.87	−1113	[54]

for those species with estimated photoionization cross sections (CH_3, CH_2CO, HCN, CH_2NH, HNCO, CH_3NO, and CH_3CN).

3. Kinetic modeling

The modeling studies for the $NH_3/CH_4/O_2$/Ar flames with R0.0, R0.1, R0.5, R0.9 and R1.0 were performed using the Premix code, which is part of the Chemkin 2.0 library [27–29]. The reaction mechanism, involving 84 species and 703 elementary reactions,

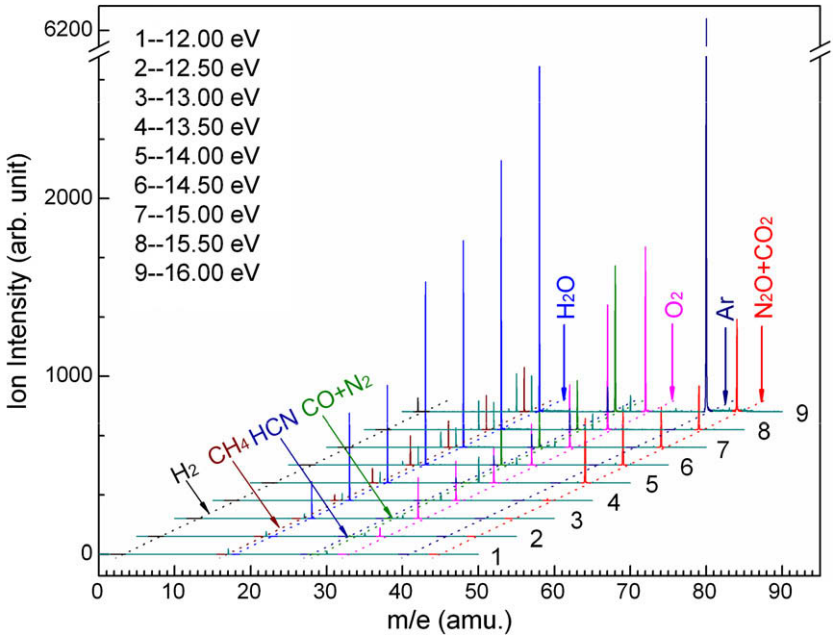

Fig. 1. Photoionization mass spectra of the $NH_3/CH_4/O_2$/Ar flame (ϕ = 1.00, *R*1.0) with different photon energies labeled on the figure, taken at the sampling position of 4.0 mm.

Table 3
Combustion species measured in the $NH_3/CH_4/O_2$/Ar flame (ϕ = 1.00, *R*1.0) along with their respective IEs.

m/e	Formula	Species	IEs (eV)	
			Literature[a]	This work[b]
2	H_2	Hydrogen	15.43	15.45
15	CH_3	Methyl radical	9.84	9.83
16	CH_4	Methane	12.78	12.77
17	NH_3	Ammonia	10.20	10.20
18	H_2O	Water	12.62	12.64
26	C_2H_2	Acetylene	11.40	11.41
27	HCN	Hydrogen cyanide	13.61	13.64
28	C_2H_4	Ethylene	10.52	10.53
	CO	Carbon monoxide	14.01	14.05
	N_2	Nitrogen	15.61	15.64
29	CH_2NH	Methanimine	9.97	10.03
30	NO	Nitric oxide	9.26	9.29
	CH_2O	Formaldehyde	10.88	10.90
	C_2H_6	Ethane	11.52	11.48
32	CH_3OH	Methyl alcohol	10.84	10.81
	O_2	Oxygen	12.13	12.15
42	CH_2CO	Ketene	9.62	9.66
43	HCNO	Fulminic acid	10.83	10.86
	HNCO	Isocyanic acid	11.60	11.57
44	CH_3CHO	Acetaldehyde	10.23	10.29
	N_2O	Nitrous oxide	12.91	12.94
	CO_2	Carbon dioxide	13.78	13.81
45	CH_3NO	Formoxime	10.59	10.54
46	NO_2	Nitrogen oxide	9.59	9.59

[a] Refers to [68].
[b] Errors for stable species are ±0.05 eV, for radicals are ±0.10 eV.

consisted of oxidation subsets for CH_4 and NH_3, together with a subset describing hydrocarbon/nitrogen interactions. The mechanism was drawn mostly from recent work on oxidation of C_1/C_2–hydrocarbons [20,30], NH_3 [14] and HCN [31], as well as interactions of these components [20,32]. In the present work a number of reactions describing hydrocarbon/amine interactions were added to the mechanism and the subsets for CH_i and NH_i radicals were updated. Table 2 lists selected reactions; the full mechanism is available in Supplementary material.

The formation of hydrocarbon radicals such as CH_2, CH and C may have a major impact on the nitrogen chemistry in methane flames. These species are very reactive and their interaction with nitrogenous species in the flame can result in formation (prompt-NO) as well as reduction (reburn type reactions) of nitrogen oxides in flames [33,34]. In addition, they may serve to convert amine species to cyanides in flames with high NH_3 concentrations. The CH_i radical subset of the mechanism was drawn mostly from Glarborg et al. [20], but a number of rate constants were updated in the present work. The key step leading from the methyl radical to methylene (CH_2) is the reaction with the hydroxyl radical. The reaction is a complex multiple well reaction with a number of potential product channels [35–40]. The reaction may lead to both triplet and singlet methylene,

$$CH_3 + OH = {}^3CH_2 + H_2O \quad (R6)$$

$$CH_3 + OH = {}^1CH_2 + H_2O. \quad (R7)$$

Here, the number refers to the list in Table 2. The CH_3 + OH reaction mainly occurs on the singlet surface and (R7) is the more important of the two steps leading to CH_2. The reaction has been measured in both the forward and reverse directions [41–43] and the data are in good agreement. In order to extrapolate these results to the low-pressure conditions of the present work, we rely on the theoretical results from Jasper et al. [39], fitting their data to obtain a set of rate coefficients at 0.04 bar.

The subsequent reactions of methylene were drawn from Glarborg et al. [20], with updates mostly from the evaluation of Baulch et al. [44]. Singlet CH_2 is rapidly converted to the triplet state by reaction with inert molecules. Even the reaction with O_2 leads almost exclusively to intersystem crossing [44]. $^3CH_2$ may be oxidized to CH_2O or CO by reaction with the O/H radical pool or with oxygen, or it may be converted to CH radicals through H-abstraction reactions. Similarly, the CH radical is oxidized to CO or HCO, or stripped of H to form atomic C.

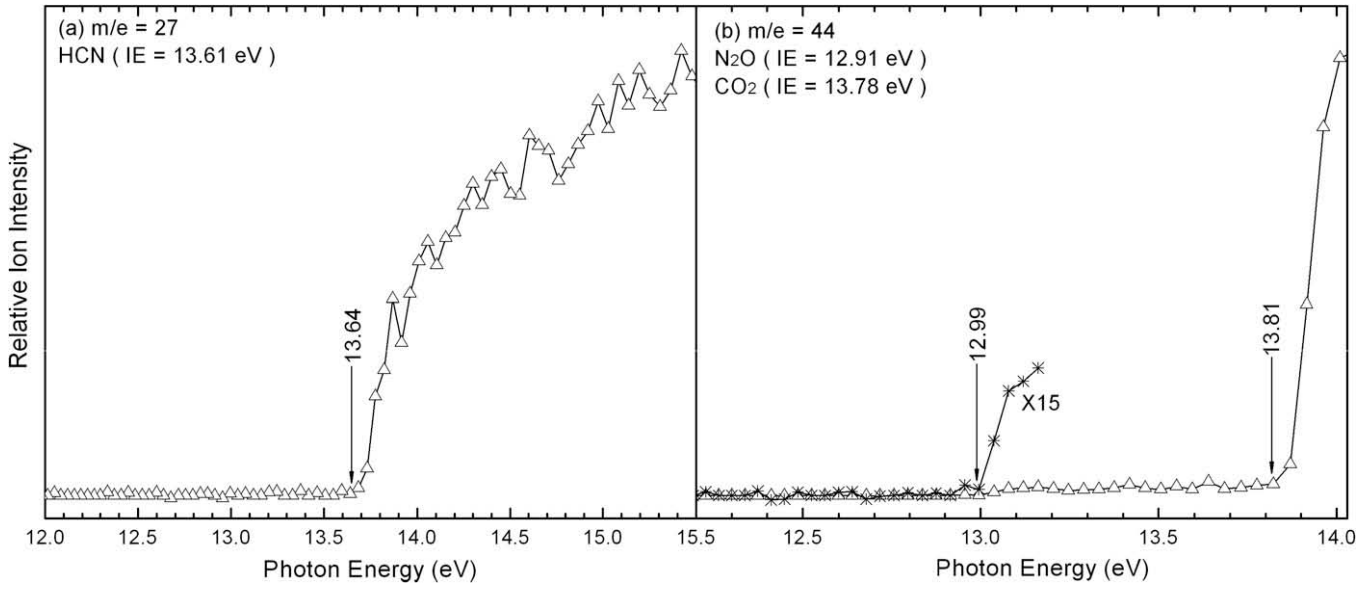

Fig. 2. Photoionization efficiency spectra of (a) $m/e = 27$ (HCN) and (b) $m/e = 44$ (N_2O/CO_2) measured in the $NH_3/CH_4/O_2/Ar$ flame ($\phi = 1.00$, $R1.0$). The accepted ionization energies for proposed species are indicated.

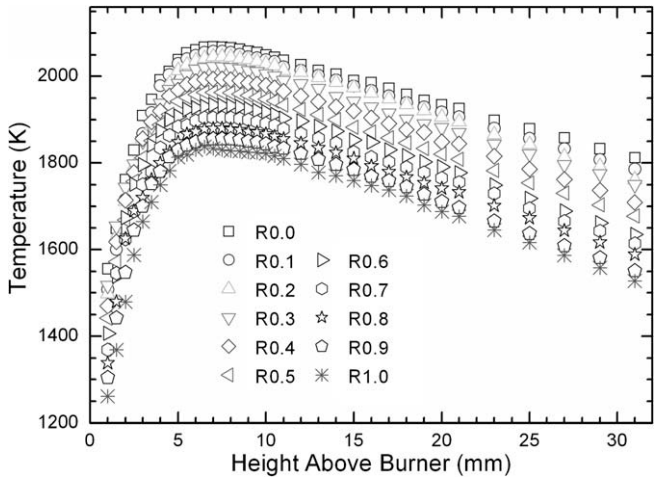

Fig. 3. Temperature profiles of the $NH_3/CH_4/O_2/Ar$ flames with different R.

Compared to the mechanism of Skreiberg et al. [14], only a few reactions were updated in the N/H/O subset (see Table 2). The fate of the NH_i radicals to a large extent determines the selectivity of NH_3 in forming NO or N_2 in the flame. These radicals may either be oxidized to NO (or HNO) by reaction with atomic oxygen or to N_2 by reaction with NO. The fate of the amine radical is determined by the local stoichiometry, temperature, and availability of reactive nitrogen species, in particular NO. The $NH_2 + O$ reaction has two major product channels,

$$NH_2 + O = HNO + H \quad (R39)$$

$$NH_2 + O = NH + OH. \quad (R40)$$

The reaction is very fast, close to collision frequency, with channel (R39) dominating. We have adopted the overall rate constant from the measurement of Inomata and Washida [45] and the branching fraction as the mean value from the measurements of Dransfeld et al. [46] and Adamson et al. [47]. Previously it was assumed that k_{39} had a negative temperature dependence [14,20,34], but the data of Inomata and Washida indicate that the rate constant is largely independent of temperature [45]. The channel going to NH + OH (R40) occurs by addition/elimination; direct abstraction is important only at very high temperatures [48].

Similarly to NH_2, NH may be oxidized to NO (or HNO), to N_2, or lose a hydrogen atom by H-abstraction. The atomic nitrogen may be oxidized to NO or react with NO to form N_2. The key reaction is

$$N + NO = N_2 + O. \quad (R41)$$

There is a substantial scatter in the measurements of k_{41} and considerable uncertainty about its temperature dependence. Baulch et al. [44] recommended a temperature independent value of $k_{41} = 2.1 \times 10^{13}$ cm^3 mol^{-1} s^{-1}, based on the study by Michael and Lim [49]. This value is consistent with the high and low temperature data within the fairly substantial scatter, notably the study of Mick et al. [50] and the flame study of Morley [51], and with the data on the reverse rate constant and the thermodynamic data within the error limits of all of these quantities. However, it should be noted that the shock tube studies of Davidson and Hanson [52] and of Koshi et al. [53] provide values that deviate from the recommendation of Baulch et al. [44] and further work on this reaction at high temperatures is desirable.

The interaction between hydrocarbons and amine species is less well established than hydrocarbon/NO interactions. The reactions may either involve H-abstraction, e.g.,

$$CH_4 + NH_2 = CH_3 + NH_3 \quad (R42)$$

$$CH_3 + NH_2 = CH_4 + NH \quad (R47)$$

$$CH_3 + NH_2 = CH_2 + NH_3 \quad (R48)$$

$$CH_3 + NH = CH_4 + N \quad (R50)$$

or feed into the methylamine/cyanide pool, e.g.,

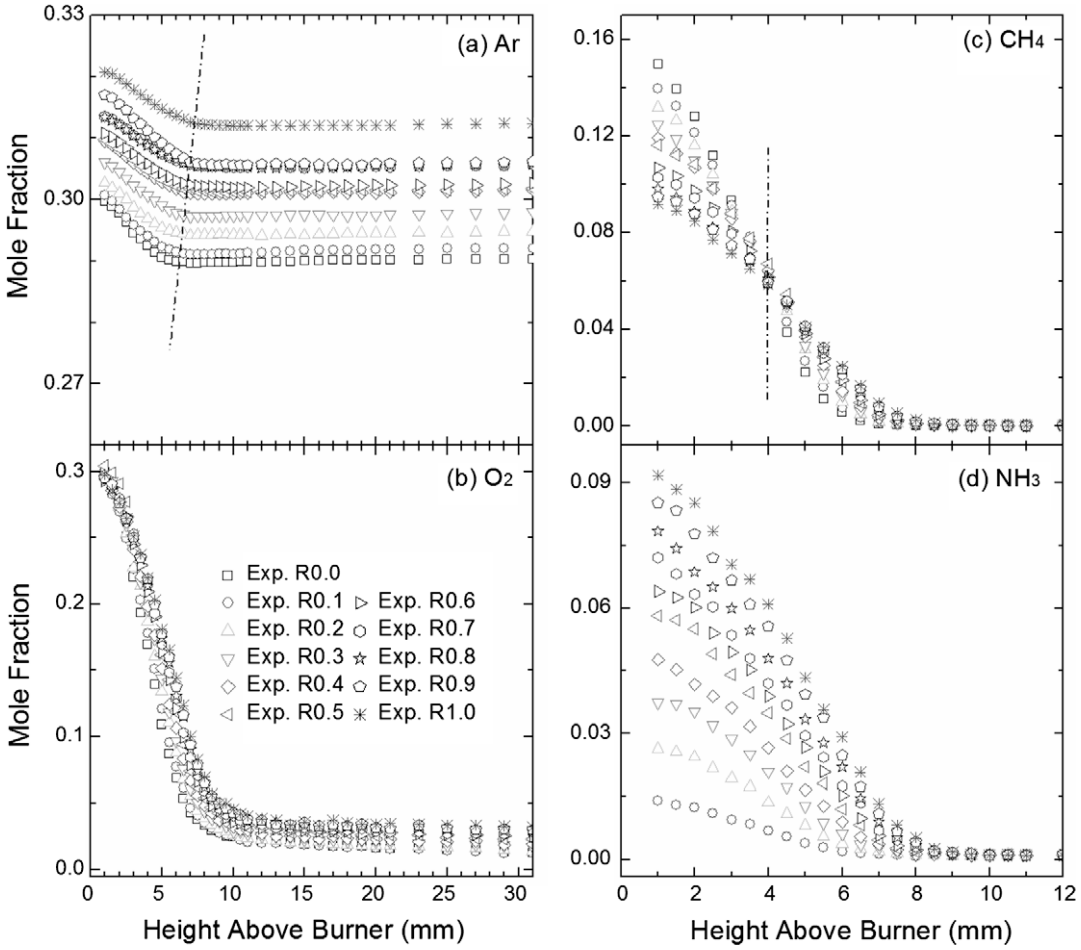

Fig. 4. Mole fraction profiles of (a) Ar, (b) O_2, (c) CH_4 and (d) NH_3 in the $NH_3/CH_4/O_2$/Ar flames with different *R*.

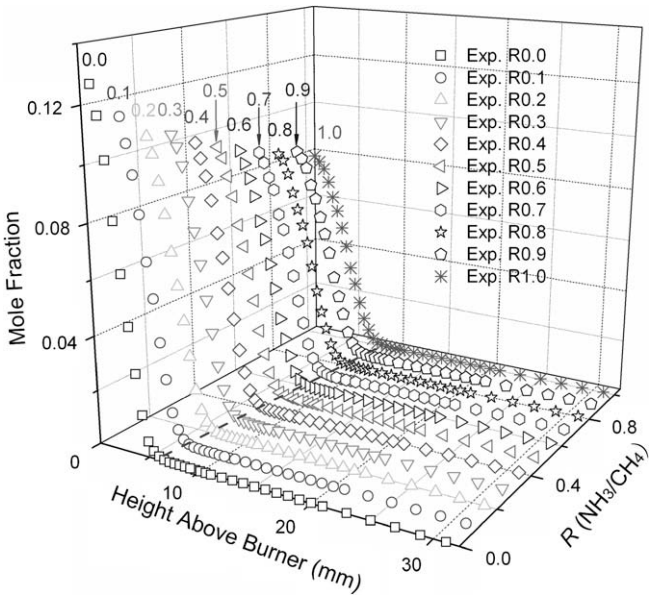

Fig. 5. Mole fraction profiles of CH_4 in the $NH_3/CH_4/O_2$/Ar flames ($\phi = 1.00$) with different *R*. The dashed line indicates the consumption point of CH_4 with the increase of *R*.

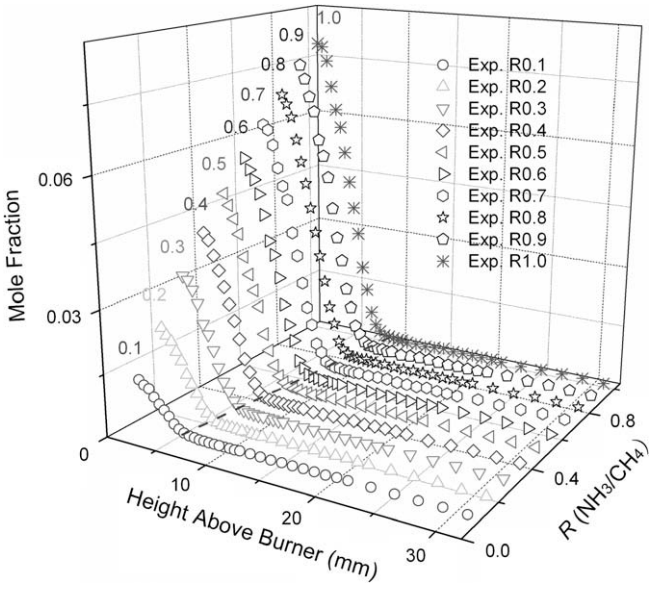

Fig. 6. Mole fraction profiles of NH_3 in the $NH_3/CH_4/O_2$/Ar flames ($\phi = 1.00$) with different *R*. The dashed line indicates the consumption point of NH_3 with the increase of *R*.

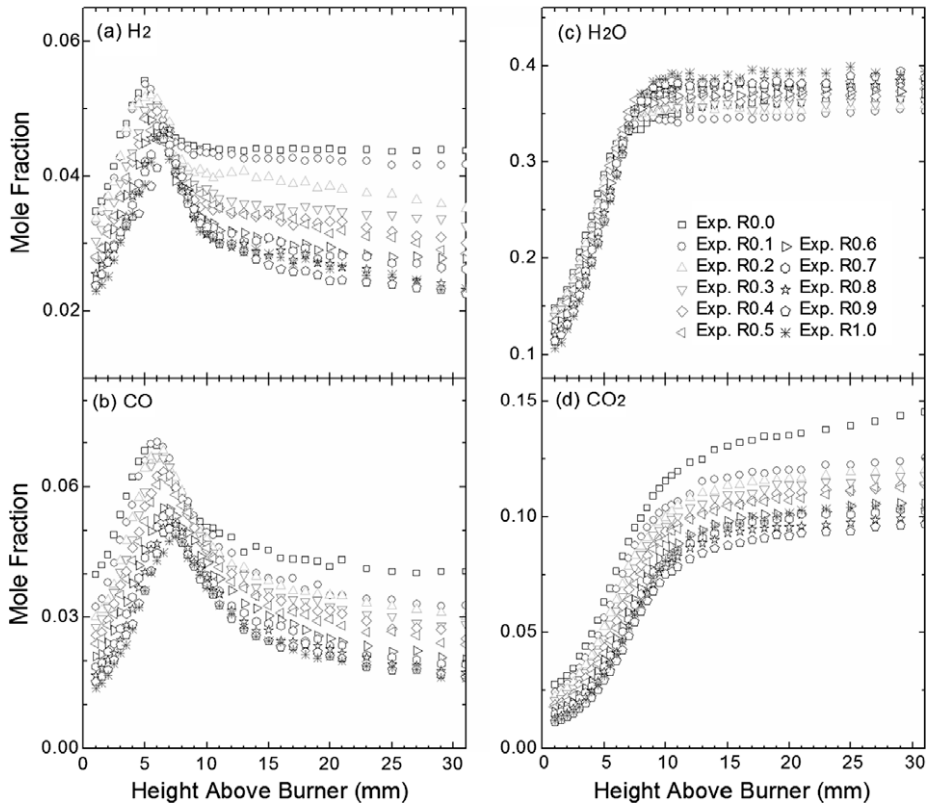

Fig. 7. Mole fraction profiles of (a) H_2, (b) CO, (c) H_2O and (d) CO_2 in the $NH_3/CH_4/O_2$/Ar flames with different *R*.

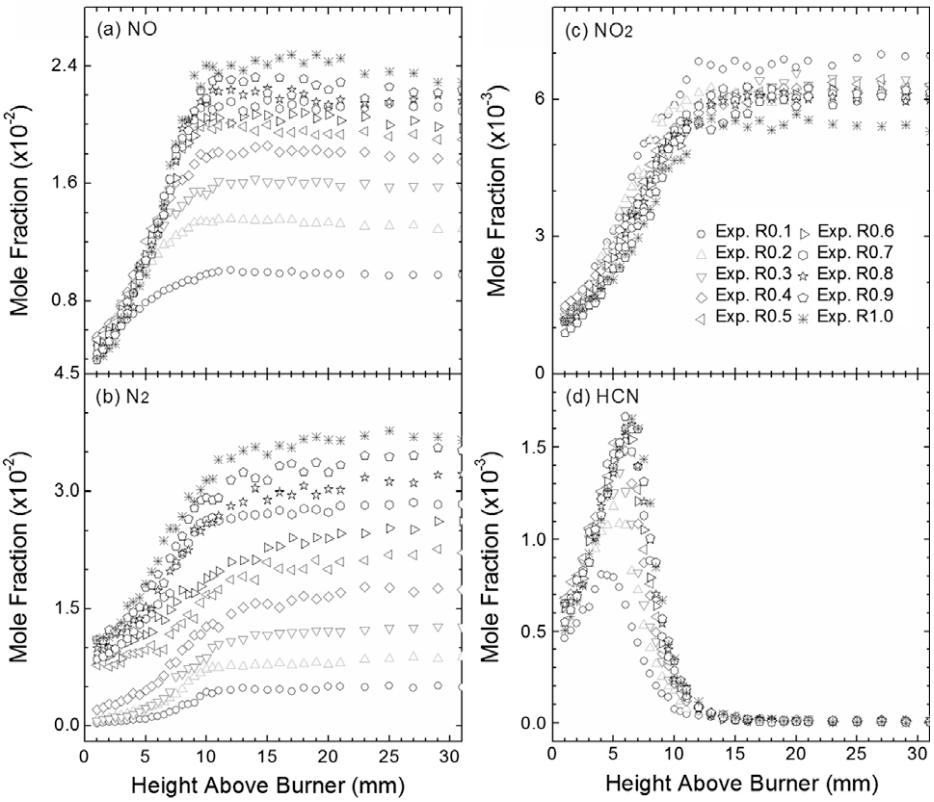

Fig. 8. Mole fraction profiles of (a) NO, (b) N_2, (c) NO_2 and (d) HCN in the $NH_3/CH_4/O_2$/Ar flames with different *R*.

$CH_3 + NH_2 = CH_3NH_2$ (R43)

$CH_3 + NH_2 = CH_2NH_2 + H$ (R44)

$CH_3 + NH = CH_2NH + H.$ (R49)

Only a few of these steps have been characterized experimentally; most rate constants were adopted from the evaluation of Dean and Bozzelli [54] and are based on QRRK estimates. The oxidation subset for methyl amine (CH_3NH_2) was also drawn largely from Dean and Bozzelli. Oxidation of CH_3NH_2 has been studied in flames [55,56], shock tubes [57–59], flow reactors [60–64], and supercritical water [65–67]. Several studies [55,57–59,64,66,67] involve a detailed reaction mechanism for CH_3NH_2 oxidation. The recent study by Shin and Yoo [59] indicates that the high-temperature ignition delay times for methylamine is fairly well predicted by the Dean and Bozzelli subset [54], but a more comprehensive validation of this chemistry is desirable.

4. Results and discussion

4.1. Identification of flame species

Fig. 1 presents the mass spectra of the $NH_3/CH_4/O_2/Ar$ flame (ϕ = 1.00, *R*1.0) at the photon energies of 12.00–16.00 eV, taken at the sampling position of 4.0 mm from the burner surface. As shown in Fig. 1, with the increase of the photon energy, the number and position of the mass peaks are changed dramatically. There are some possible isomers for each mass and the total number of isomers increases rapidly with the increase of molecular weight. Thus, identification of these isomeric intermediates by measurements of PIE spectra is desired. The tunable photon energy from synchrotron allows unambiguous measurements of PIE spectra for each observed mass.

In this study, about 20 flame species are detected and identified, which are listed in Table 3 along with literature IEs [68]. Two PIE spectra are selected for illustration here. Fig. 2 displays the PIE spectra of HCN and N_2O/CO_2. Among these species, though acetylene (C_2H_2), ethylene (C_2H_4), methanimine (CH_2NH), ketene (CH_2CO), fulminic acid (HCNO), isocyanic acid (HNCO), acetaldehyde (CH_3CHO) and formoxime were reported in other nitrogenous compounds flames [26,69–71], they have not been detected in previous experimental studies of $NH_3/CH_4/O_2$ flames [2,3,6,7].

4.2. Effect of R on temperature and mole fraction profiles

4.2.1. Temperature profiles

The temperature profiles of the 11 flames are shown in Fig. 3. The temperature profiles of the investigated flames have similar tendencies. With *R* increasing, the flame temperatures decrease gradually, as a result of the reduction of CH_4. The maximum temperature is 2068 K measured in the flame *R*0.0, which is approximately 230 K higher than that of the flame *R*1.0.

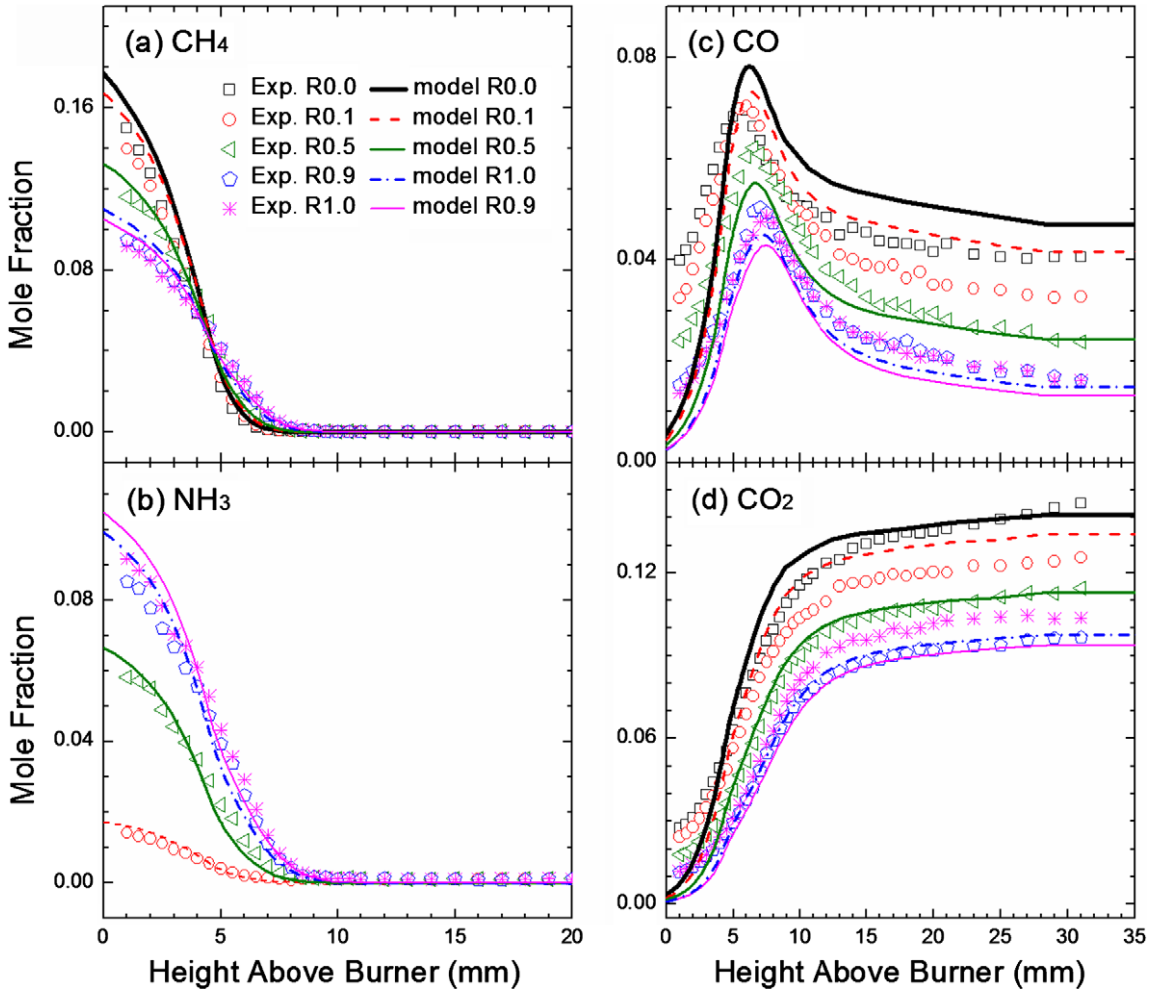

Fig. 9. Mole fraction profiles of the major species (a) CH_4, (b) NH_3, (c) CO and (d) CO_2 for the flames *R*0.0, *R*0.1, *R*0.5, *R*0.9 and *R*1.0. Symbols and lines correspond to experimental and simulation results, respectively.

4.2.2. Mole fraction profiles

Mole fraction profiles of Ar and the reactants (O_2, CH_4 and NH_3) are illustrated in Fig. 4. With *R* increasing, the mole fraction profiles of Ar and O_2 change slightly while CH_4 and NH_3 are consumed further downstream in the flame. In the flame *R*0.0, the mole fraction of Ar remains constant after the position of 6.5 mm from the burner surface. This position shifts downstream with *R* increasing and reaches 8.0 mm with the flame *R*1.0, indicating that the reaction zone is broadened as *R* increasing. CH_4 is consumed completely before 12 mm in all investigated flames. A turning point at about 4 mm is observed. For a specific burner distance, concentration of CH_4 has a decreasing trend with *R* increasing before this turning point but a reverse trend after the point, showing that the reaction zone is widened, which is in agreement with the conclusion based on the Ar mole fraction profiles. The 3D mole fraction profiles of CH_4 and NH_3 with the different *R* are illustrated in Figs. 5 and 6. The dashed lines correspond to the consumption distances of CH_4 and NH_3. With *R* increasing, the distances shift downstream for both CH_4 and NH_3.

Figs. 7 and 8 display mole fraction profiles of H_2, CO, H_2O, CO_2, NO, N_2, NO_2 and HCN. As a typical of intermediate species, H_2 has peak-shaped mole fraction profiles in all investigated flames. With *R* increasing, the maximum mole fraction decreases and the peak position shifts downstream. This observation is different from the results of Puechberty and Cottereau [2], who reported a maximum concentration of H_2 at the burner surface. For H_2O, the tendency for the position with equilibrium value is similar to that of Ar. However, its value in the post-flame zone is slightly increased, which is contrary to that of Ar. *R* has the same effect on CO as that on H_2. The peak mole fraction of CO in the flame without NH_3 is 7.0×10^{-2} at 5.5 mm, while in the flame *R*1.0, this value decreases to 4.9×10^{-2} at 7.5 mm. The reduction of the CO concentration results from the reduced amount of CH_4. A similar trend is seen for CO_2. For the major nitrogenous products, the quantities of NO and N_2 increase with *R* increasing, while the concentration of NO_2 decreases. In each flame, the order of concentration is NO > N_2 > NO_2 when *R* is lower than 0.7, which is in good agreement with the results reported by Puechberty and Cottereau [2] and Garo et al. [6]. For the flames with $R \geqslant 0.7$, an order of N_2 > NO > NO_2 is observed. The fact that NO_2 decreases with *R* increasing is expected, since the methyl radical is effective in reducing NO_2 to NO [72].

Mole fractions of a range of hydrocarbon and nitrogenous intermediates in all flames have been detected, and HCN is selected for illustration on experimentally observed trends. As shown in Fig. 8(d), the maximum mole fraction of HCN is 8.10×10^{-4} at 4.5 mm in the flame *R*0.1. This value increases to 1.18×10^{-3} at 5.0 mm in the flame *R*0.2. This effect becomes more obvious with *R* increasing, for example, the peak mole fraction of HCN is 1.66×10^{-3} at 6.5 mm in the flame *R*1.0.

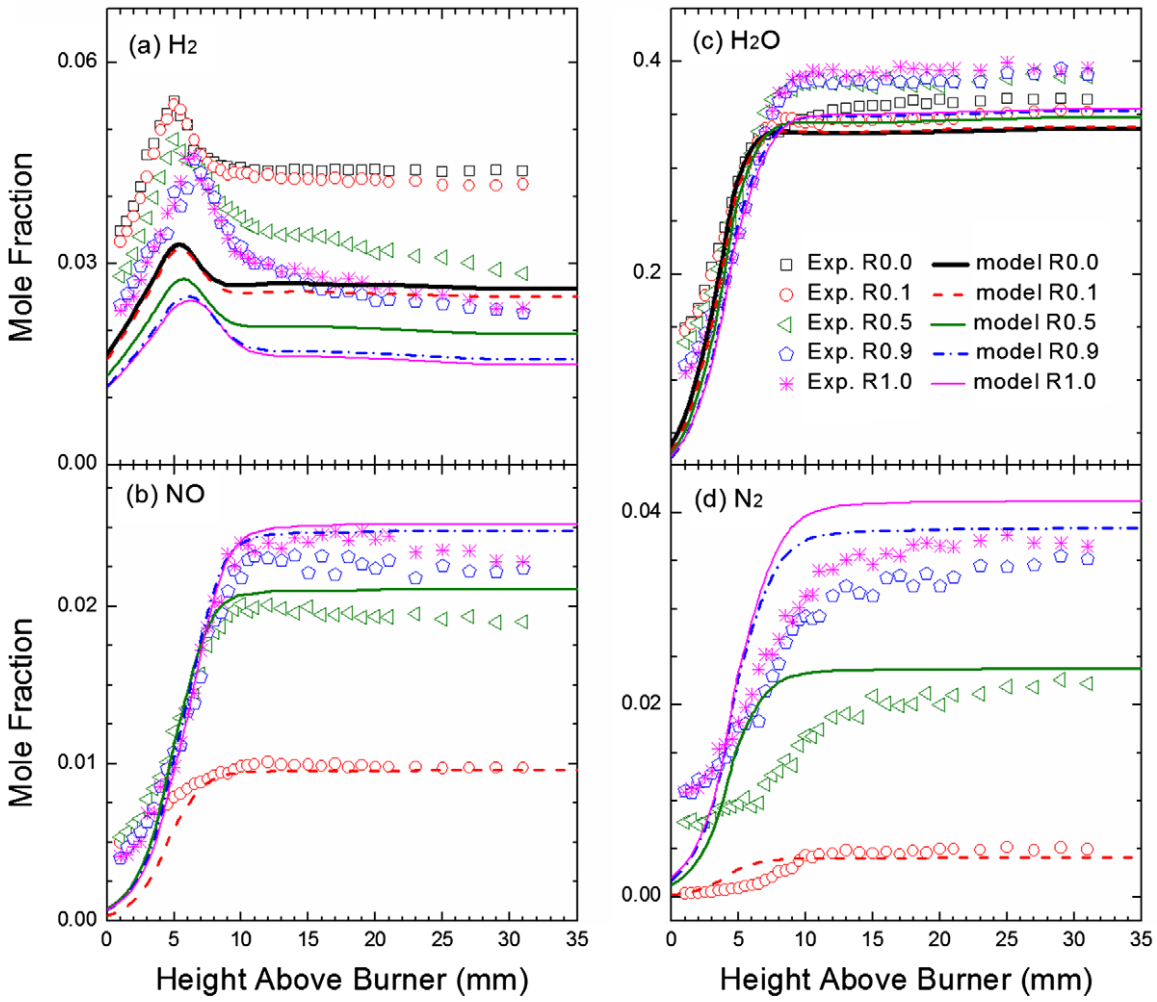

Fig. 10. Mole fraction profiles of the major species (a) H_2, (b) NO, (c) H_2O and (d) N_2 for the flames *R*0.0, *R*0.1, *R*0.5, *R*0.9 and *R*1.0. Symbols and lines correspond to experimental and simulation results, respectively.

4.3. Comparison between experimental results and modeling predictions

In the following, the measured flame profiles are compared with modeling results, using the reaction mechanism discussed in Section 3. Five flames, i.e. *R*0.0, *R*0.1, *R*0.5, *R*0.9 and *R*1.0, are selected for comparison. The experimental temperature profiles were used in the calculations. However, to account for the perturbations induced by the quartz probe and the thermocouple, the temperature profiles were shifted 2.0 mm away from the burner surface in this work. The perturbation effect is known in molecular-beam mass spectroscopic investigations, and a shift equaling 4–5 times the orifice diameter has been reported for premixed low-pressure flames (4.4–5.0 kPa) [24,73–77].

Figs. 9 and 10 compare the predicted and experimental mole fraction profiles of the major species in the selected flames. Here, as well as in the following figures, symbols denote experimental results and lines correspond to simulations. As shown in Fig. 9(a) and (b), the modeling result reproduces satisfactorily the consumption of the reactants. The intersection at 4.0 mm in the experimental results of CH_4 is also observed in that of the computed profiles. For CO, both the experiments and the simulations show that the peak concentration is decreased and the corresponding position is shifted downstream with *R* increasing. A satisfactory agreement is observed between the experimental and predicted mole fraction profiles of CO_2. For H_2 and H_2O (see Fig. 10), the mechanism predicts the same tendency as the experiments, although it underpredicts the absolute concentrations for the same *R*. The formation of the major nitrogenous products, NO and N_2 is also correctly simulated by the model.

Figs. 11 and 12 compare the experimental and modeling mole fraction profiles of CH_3, C_2H_2, C_2H_4, CH_2CO, HCN, CH_2NH, HNCO, CH_3NO and CH_3CN for the flame *R*1.0. In general, the modeling predictions for these species are in good agreement with the experimental results. Generally, the location of the peak concentration in the calculations is slightly shifted (1–2 mm) downstream, but for most of the species the peak value is predicted well. In particular, it is noteworthy that the nitrogenous intermediates HCN, HNCO and CH_2NH are well predicted by the model, supporting the validity of the present reaction mechanism. Reactions related to the formation and consumption of, e.g., CH_2NH, CH_3NO and CH_3CN were not considered in the previous mechanisms by Skreiberg et al. [14], Miller and Bowman [34] or GRI-MECH 3.0 [78], but as discussed below these species have only a limited impact on the formation of NO in the current flames.

4.4. Flow rate and sensitivity analysis

For brevity, we discuss here only the flow rate analysis of CH_4 and NH_3 oxidation in the flame *R*1.0. Fig. 13 is based on the predicted rate-of-production coefficients. The initial steps of CH_4 oxidation are the reaction of CH_4 with OH and H, forming CH_3. The methyl radical is mainly converted to singlet CH_2 by reacting with OH (R7/SR71) and CH_2O by O-addition (R4/SR68), in good agreement with the specification mentioned in the kinetic modeling section. Singlet CH_2 transforms rapidly to triplet CH_2 (R23,R27/SR92–SR96), which can react with H, OH and CH_3 to form CH, CH_2O and C_2H_4 (R13/SR81, R16/SR84 and SR174). Formaldehyde reacts mainly with OH radical to give HCO (SR47), which leads predominantly to the production of H_2 and CO (SR50–SR52, SR54 and

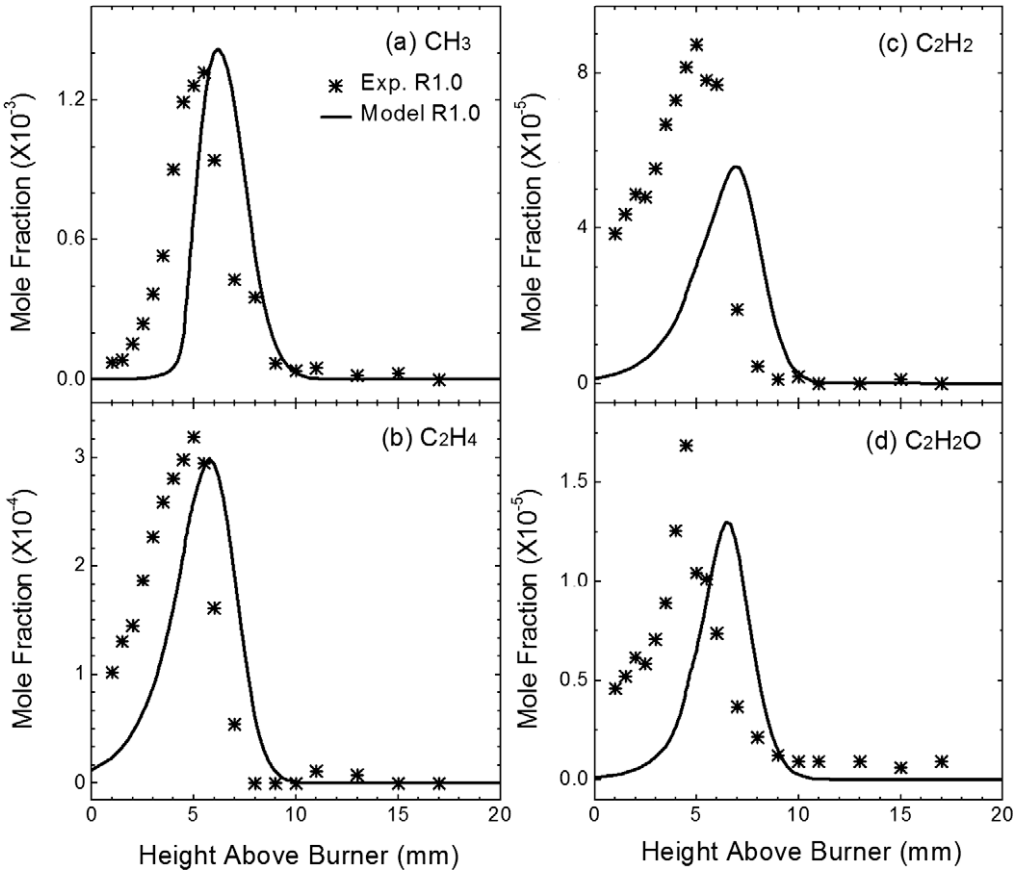

Fig. 11. Mole fraction profiles of (a) CH_3, (b) C_2H_4, (c) C_2H_2 and (d) C_2H_2O in the flame *R*1.0. Symbols and lines correspond to experimental and simulation results, respectively.

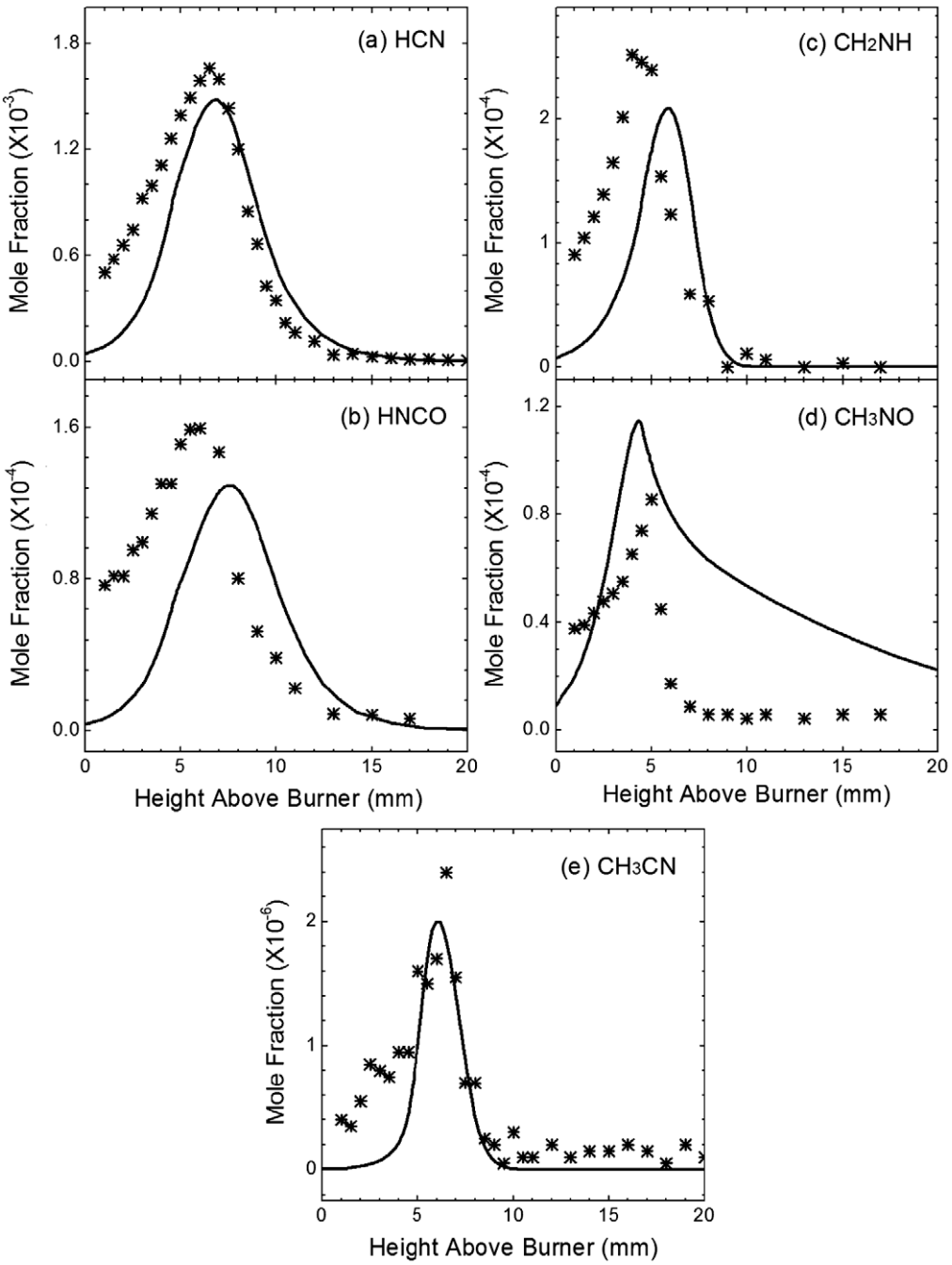

Fig. 12. Mole fraction profiles of (a) HCN, (b) HNCO, (c) CH_2NH, (d) CH_3NO and (e) CH_3CN in the flame *R*1.0. Symbols and lines correspond to experimental and simulation results, respectively.

SR55). CH is another precursor of HCO (R34/SR106). In addition, CH can react with NO to generate HCN (SR614), which accounts for 10% of HCN production.

The NH_3 consumption is initiated through the reaction with OH to produce NH_2 (SR354). The NH_2 radical is mainly converted to HNO (SR357) and NH (SR356 and SR360), both of which are important precursors of NO. Besides forming NO, NH can react with NO and H to give N_2O (SR383) and N (SR375), respectively, both of which may yield either NO or N_2. Most of the NO is formed from the reaction HNO + H = NO + H_2 (SR304) (54% contribution) while HNO + OH = NO + H_2O (SR306) and NH + O = NO + H (SR376) are secondary formation pathways. The main consumption channels of NO are reactions with NH_i, leading to the formation of N_2O (SR383) and N_2 (SR370, SR385 and SR390). These major pathways are in line with earlier studies [1,34].

Minor pathways of NH consumption include reacting with OH and CH_3 to produce HNO (6% consumption, SR377) and CH_2NH (9% consumption, SR583). CH_2NH can convert to H_2, CO and HCN and CH_3CN through the reaction sequences $CH_2NH \rightarrow CH_2O$ (SR675) → HCO (SR47) → H_2, CO (SR50–SR52, SR54 and SR55) and $CH_2NH \rightarrow H_2CN$ (SR673 and SR676), HCNH (SR674 and SR677) → HCN (SR682 and SR691). The reaction $CH_3 + NO \rightarrow HCN + H_2O$ has been postulated as a dominant route for the formation of HCN [34,79–81]. However, the flow rate analysis indicates that under the present conditions HCN is formed predominantly by the decomposition of HCNH and H_2CN. As mentioned above, reaction SR614 is another source of

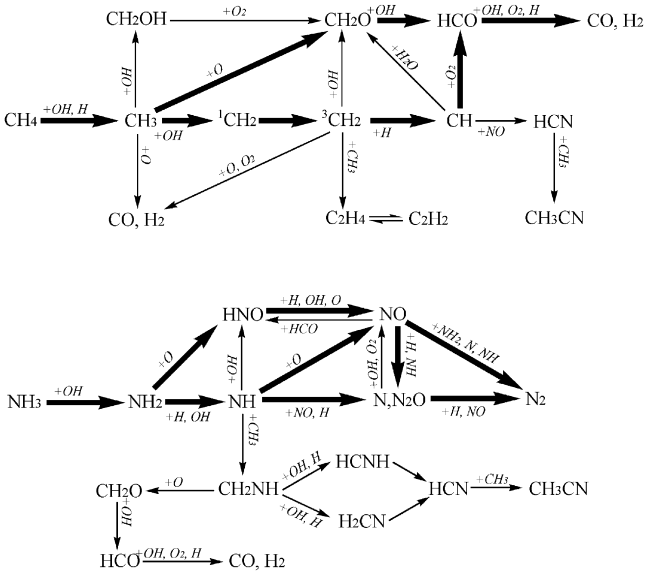

Fig. 13. Flow rate analysis of the consumption of CH_4 and NH_3 at the distance of 7.0 mm from the burner surface in the flame *R*1.0.

HCN, which is in agreement with previous studies [34,55]. According to Miller and Bowman, HCN converts mainly to NH_i, CN, NCO and HNCO through the reactions with O/OH [34]. However, the flow rate analysis shows that NCO (SR469), HNC (SR467), CH_3CN (SR698), CN (SR472) are its major products. It should be noted that few reactions of the smaller hydrocarbon radicals such as CH_2 and CH show up in the flow rate analysis of NH_3 oxidation, indicating that they play only a minor role under the conditions of the present flames.

To identify the reactions that serve as bottle-necks in the formation of NO, a local sensitivity analysis has been performed with the proposed mechanism for the flames *R*0.1, *R*0.5 and *R*1.0, as shown in Fig. 14. The sensitivity analysis shows that, in all cases, reactions $H + O_2 = O + OH$ (SR1, i.e. the reaction 1 in Supplemental material) and $NH_2 + O = HNO + H$ (R39/SR357) play key roles for NO formation while $NH_2 + NO = N_2 + H_2O$ (SR370) and $NH + NO = N_2O + H$ (SR383) are important for NO consumption, indicating that the importance of these reactions do not depend much on *R*. In comparison, reactions $NH + O = NO + H$ (SR376), $HCO = H + CO$ (SR50), $NH + OH = HNO + H$ (SR377), $N + OH = NO + H$ (SR388), $NH_2 + NO = NNH + OH$ (SR371), $NH_2 + H = NH + H_2$ (SR356), $NH_3 + OH = NH_2 + H_2O$ (SR354) and $CH_3 + O = CH_2O + H$ (R4/SR68) have less effect on the formation of NO. With *R* increasing, most of the reactions listed in the figure exhibit higher absolute sensitivity coefficients (SC), showing that the

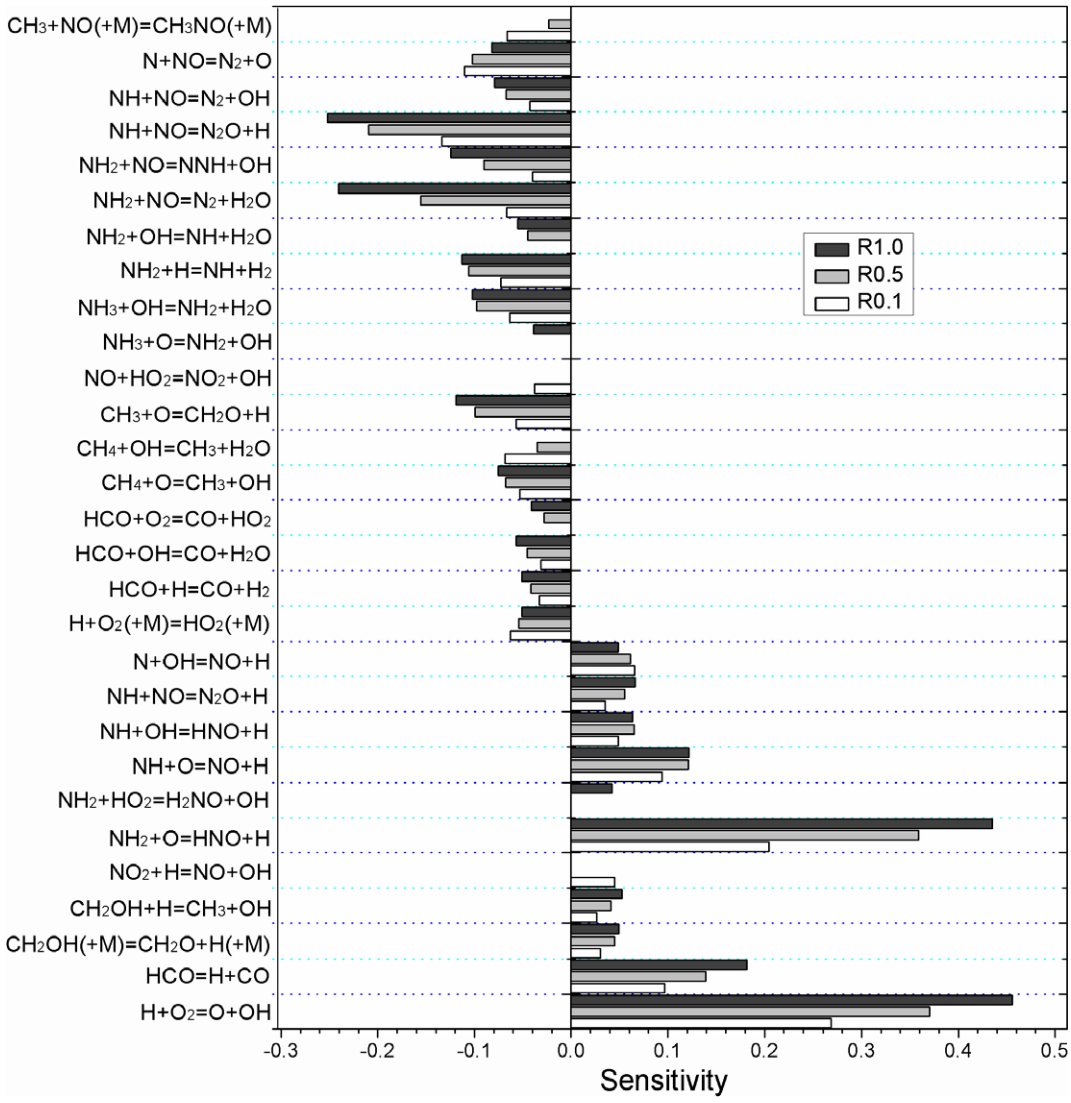

Fig. 14. Sensitivity analysis of the conversion of NO in the flames *R*0.1, *R*0.5 and *R*1.0 (only the reactions with an absolute value of the sensitivity coefficient higher than 0.035 are considered).

promoting and inhibiting effect are increased for those reactions with positive and negative SC, respectively. However, for the reactions SR388, $NO_2 + H = NO + OH$ (SR315), $CH_3 + NO (+M) = CH_3NO (+M)$ (SR550), $N + NO = N_2 + O$ (R41/SR390), $CH_4 + OH = CH_3 + H_2O$ (SR61) and $H + O_2 (+M) = HO_2 (+M)$ (SR7) their importance decreases with increasing values of *R*. Similar to the situation of NO, conversion of N_2 is highly sensitive to SR1, R39/SR357, SR370 and SR383 for all three flames (see Fig. S4 in Supplemental material). In addition, reactions SR354 and SR371 also show high SC. With *R* increasing, most of the reactions show lower absolute SC, which is contrary to those of NO. It is noteworthy that both the predicted NO and N_2 show little sensitivity towards interactions between hydrocarbon and nitrogen species. Specifically, none of the hydrocarbon/amine reactions show up in the analysis. Neither do reactions of stable nitrogen intermediates such as HCN, CH_2NH and HNCO, even though they are present in considerable concentrations. These results are in line with the findings of Glarborg et al. [1] that in flames containing volatile reactive nitrogen compounds, the selectivity for forming NO or N_2 is largely determined by the fate of the small amine radicals.

5. Conclusions

Eleven low-pressure premixed $NH_3/CH_4/O_2/Ar$ flames at equivalence ratio of 1.0 have been investigated experimentally with tunable synchrotron VUV photoionization and molecular-beam mass spectrometry. Combustion intermediates and products are identified by measurements of photoionization efficiency spectra. Mole fractions of the flame species are calculated and flame temperatures are measured by a Pt/Pt–13%Rh thermocouple. The experimental data of the flames *R*0.0, *R*0.1, *R*0.5, *R*0.9 and *R*1.0 are compared with the results of kinetic modeling using an updated reaction mechanism. The reaction mechanism is composed of 84 species and 703 elementary reactions. The experimental results indicate that the reaction zone is widened with *R* increasing; the mole fraction profiles of H_2O, NO and N_2 ascend while those profiles of H_2, CO, CO_2 and NO_2 have reverse tendencies. The computational result shows that the proposed mechanisms can correctly predict the concentration profiles of the major species and intermediates. Moreover, sensitivity and flow rate analyses have been performed to demonstrate the key reactions in the mechanism. Among the reactions, $H + O_2 = O + OH$, $NH_2 + O = HNO + H$, $NH_2 + NO = N_2 + H_2O$ and $NH + NO = N_2O + H$ play significant roles for NO and N_2 conversion; CH_3, $^1CH_2$, $^3CH_2$, CH_2O, NH_2, NH and HNO are the key species in the oxidation of CH_4 and NH_3.

Acknowledgments

F.Q. is grateful for the funding supports from Chinese Academy of Sciences, Natural Science Foundation of China under Grant No. 20533040, National Basic Research Program of China (973) under Grant No. 2007CB815204 and Ministry of Science and Technology of China under Grant No. 2007DFA61310. P.G. acknowledges support from Energinet DK under Grant PSO 4806. The authors thank Dr. Frederique Battin-Leclerc, Dr. Jing Wang, Mr. Tao Yuan, Ms. Xin Hong, Mr. Taichang Zhang, Mr. Kuiwen Zhang and Dr. Ahren Jasper for their helpful discussions.

Appendix A. Supplementary data

1. The detailed reaction mechanism of the premixed $NH_3/CH_4/O_2/Ar$ flames at low pressure.
2. Effect of a temperature deviation on modeling results.
3. Sensitivity analysis of the conversion of N_2.

Supplementary data associated with this article can be found, in the online version, at doi:10.1016/j.combustflame.2009.03.005.

References

[1] P. Glarborg, A.D. Jensen, J.E. Johnsson, Prog. Energy Combust. Sci. 29 (2003) 89–113.
[2] D. Puechberty, M.J. Cottereau, Combust. Flame 51 (1983) 299–311.
[3] B. Rosier, P. Gicquel, D. Henry, A. Coppalle, Appl. Opt. 27 (1988) 360–364.
[4] J. Bian, J. Vandooren, P.J.V. Tiggelen, Proc. Combust. Inst. 21 (1986) 953–963.
[5] J. Bian, J. Vandooren, P.J.V. Tiggelen, Proc. Combust. Inst. 23 (1990) 379–386.
[6] A. Garo, C. Hilaire, D. Puechberty, Combust. Sci. Technol. 86 (1992) 87–103.
[7] B.A. Williams, J.W. Fleming, Combust. Flame 100 (1995) 571–590.
[8] N. Sullivan, A. Jensen, P. Glarborg, M.S. Day, J.F. Grcar, J.B. Bell, C.J. Pope, R.J. Kee, Combust. Flame 131 (2002) 285–298.
[9] I. Rahinov, A. Goldman, S. Cheskis, Combust. Flame 145 (2006) 105–116.
[10] I.V. Dyakov, A.A. Konnov, J.D. Ruyck, Khim. Fiz. 23 (2004) 19–24.
[11] R.C. Sausa, G. Singh, G.W. Lemire, W.R. Anderson, Proc. Combust. Inst. 26 (1996) 1043–1052.
[12] D.T. Venizelos, R.C. Sausa, Combust. Flame 115 (1998) 313–326.
[13] A.A. Konnov, I.V. Dyakov, J.D. Ruyck, Combust. Sci. Technol. 178 (2006) 1143–1164.
[14] Ø. Skreiberg, P. Kilpinen, P. Glarborg, Combust. Flame 136 (2004) 501–518.
[15] C.A. Taatjes, N. Hansen, A. McIlroy, J.A. Miller, J.P. Senosiain, S.J. Klippenstein, F. Qi, L.S. Sheng, Y.W. Zhang, T.A. Cool, J. Wang, P.R. Westmoreland, M.E. Law, T. Kasper, K. Kohse-Höinghaus, Science 308 (2005) 1887–1889.
[16] B. Yang, Y.Y. Li, L.X. Wei, C.Q. Huang, J. Wang, Z.Y. Tian, L.S. Liu, Y.W. Zhang, F. Q, Proc. Combust. Inst. 31 (2006) 555–563.
[17] B. Yang, P. Oβwald, Y.Y. Li, J. Wang, L.X. Wei, Z.Y. Tian, F. Qi, K. Kohse-Höinghaus, Combust. Flame 148 (2007) 198–209.
[18] F. Qi, R. Yang, B. Yang, C.Q. Huang, L.X. Wei, J. Wang, L.S. Sheng, Y.W. Zhang, Rev. Sci. Instrum. 77 (2006) 084101.
[19] C.Q. Huang, L.X. Wei, B. Yang, J. Wang, Y.Y. Li, L.S. Sheng, Y.W. Zhang, F. Qi, Energy Fuels 20 (2006) 1505–1513.
[20] P. Glarborg, M.U. Alzueta, K. Dam-Johansen, Combust. Flame 115 (1998) 1–27.
[21] H.A. Moneib, Experimental study of the fluctuating temperature in inert and reacting turbulent jets, Doctorate Thesis, Imperial College of Science and Technology, 1980.
[22] C.A. Martins, A.P. Pimenta, J.A. Carvalho, M.A. Ferreira, A.A. Caldeira-Pires, J. Braz. Soc. Mech. Sci. Eng. 27 (2005) 110–118.
[23] R.M. Fristrom, Flame Structure and Processes, Oxford, New York, 1995. pp. 118–119.
[24] A. Bhargava, P.R. Westmoreland, Combust. Flame 113 (1998) 333–347.
[25] M. Kamphus, N.N. Liu, B. Atakan, F. Qi, A. McIlroy, Proc. Combust. Inst. 29 (2002) 2627–2633.
[26] Z.Y. Tian, L.D. Zhang, Y.Y. Li, T. Yuan, F. Qi, Proc. Combust. Inst. 32 (2009) 311–318.
[27] R.J. Kee, J.F. Grcar, M.D. Smooke, J.A. Miller, Sandia Report: SAND85-8240, 1985.
[28] R.J. Kee, F.M. Rupley, J.A. Miller, Sandia Report: SAND89-8009B, 1989.
[29] J.C. Grcar, R.J. Kee, M.D. Smooke, J.A. Miller, Proc. Combust. Inst. 21 (1986) 1773–1782.
[30] C.L. Rasmussen, J.G. Jacobsen, P. Glarborg, Int. J. Chem. Kinet. 40 (2008) 778–807.
[31] P. Dagaut, P. Glarborg, M.U. Alzueta, Prog. Energy Combust. Sci. 34 (2008) 1–46.
[32] C.L. Rasmussen, P. Glarborg, Combust. Flame 154 (2008) 529–545.
[33] P. Glarborg, R.J. Kee, J.A. Miller, Combust. Flame 65 (1986) 177–202.
[34] J.A. Miller, C.T. Bowman, Prog. Energy Combust. Sci. 15 (1989) 287–338.
[35] A.M. Dean, P.R. Westmoreland, Int. J. Chem. Kinet. 19 (1987) 207–228.
[36] R. Humpfer, H. Oser, H.H. Grotheer, T. Just, Proc. Combust. Inst. 25 (1994) 721–731.
[37] R.D.A. Pereira, D.L. Baulch, M.J. Pilling, S.H. Robertson, G. Zeng, J. Phys. Chem. A 101 (1997) 9681–9693.
[38] R. Deters, M. Otting, H.G. Wagner, F. Temps, B. Laszlo, S. Dobe, T. Berces, Ber. Bunsenges. Phys. Chem. 102 (1998) 58–72.
[39] A.W. Jasper, S.J. Klippenstein, L.B. Harding, B. Ruscic, J. Phys. Chem. A 111 (2007) 3932–3950.
[40] N.K. Srinivasan, M.C. Su, J.V. Michael, J. Phys. Chem. A 111 (2007) 3951–3958.
[41] W. Hack, H.G. Wagner, A. Wilms, Ber. Bunsenges. Phys. Chem. 92 (1988) 620–627.
[42] H.H. Carstensen, H.G. Wagner, Ber. Bunsenges. Phys. Chem. 99 (1995) 1539–1545.
[43] L.N. Krasnoperov, J.V. Michael, J. Phys. Chem. A 108 (2004) 8317–8323.
[44] D.L. Baulch, C.T. Bowman, C.J. Cobos, R.A. Cox, T. Just, J.A. Kerr, M.J. Pilling, D. Stocker, J. Troe, W. Tsang, R.W. Walker, J. Warnatz, J. Phys. Chem. Ref. Data 34 (2005) 757–1397.
[45] S. Inomata, N. Washida, J. Phys. Chem. A 103 (1999) 5023–5031.
[46] P. Dransfeld, W. Hack, H. Kurzke, F. Temps, H.G. Wagner, Proc. Combust. Inst. 20 (1984) 655–664.
[47] J.D. Adamson, S.K. Farhat, C.L. Morter, G.P. Glass, R.F. Curl, L.F. Philips, J. Phys. Chem. 98 (1994) 5665–5669.

[48] X.F. Duan, M. Page, J. Chem. Phys. 102 (1995) 6121–6127.
[49] J.V. Michael, K.P. Lim, J. Chem. Phys. 97 (1992) 3228–3234.
[50] H.J. Mick, H. Matsui, P. Roth, J. Phys. Chem. 97 (1994) 6839–6842.
[51] C. Morley, Proc. Combust. Inst. 18 (1981) 23–32.
[52] D.F. Davidson, R.K. Hanson, Int. J. Chem. Kinet. 22 (1990) 843–861.
[53] M. Koshi, M. Yoshimura, K. Fukuda, M. Matsui, K. Saito, M. Watanabe, A. Imamura, C. Chen, J. Chem. Phys. 93 (1990) 8703–8708.
[54] A.M. Dean, J.W. Bozzelli, Combustion chemistry of nitrogen, in: W.C. Gardiner Jr. (Ed.), Gas-Phase Combustion Chemistry, Springer, NY, 2000, pp. 125–341.
[55] B.A. Williams, J.W. Fleming, Combust. Flame 110 (1997) 1–13.
[56] K. Takizawa, A. Takahashi, K. Tokuhashi, S. Kondo, A. Sekura, J. Haz. Mat. 155 (2008) 144–152.
[57] T. Higashihara, W.C. Gardiner Jr., S.M. Hwang, J. Phys. Chem. A 91 (1987) 1900–1905.
[58] S.M. Hwang, T. Higashihara, K.S. Shin, W.C. Gardiner Jr., J. Phys. Chem. A 94 (1990) 2883–2889.
[59] K.S. Shin, S.J. Yoo, Bull. Korean Chem. Soc. 25 (2004) 293–297.
[60] V.Y. Basevich, S.M. Kogarko, A.M. Tyurin, Khim. Fiz. 2 (1983) 113.
[61] V.Y. Basevich, Prog. Energy Combust. Sci. 13 (1987) 199–248.
[62] K. Hjuler, P. Glarborg, K. Dam-Johansen, Ind. Eng. Chem. Res. 34 (1995) 1882–1888.
[63] F.H. Mao, R.B. Barat, Combust. Flame 105 (1996) 557–568.
[64] M.V. Kantak, K.S.D. Manrique, R.H. Aglave, R.P. Hesketh, Combust. Flame 108 (1997) 235–265.
[65] K.M. Benjamin, P.E. Savage, Ind. Eng. Chem. Res. 44 (2005) 5318–5324.
[66] K.M. Benjamin, P.E. Savage, Ind. Eng. Chem. Res. 44 (2005) 9785–9793.
[67] H. Li, Y. Oshima, Ind. Eng. Chem. Res. 44 (2005) 8756–8764.
[68] P.J. Linstrom, W.G. Mallard, in: P.J. Linstrom, W.G. Mallard (Eds.), NIST Chemistry Webbook, NIST Standard Reference Database Number 69, June 2005, National Institute of Standards and Technology, Gaithersburg, MD 20899. Available from: <http://webbook.nist.gov/chemistry>.
[69] A. Lucassen, P. Oβwald, U. Struckmeier, K. Kohse-Höinghaus, T. Kasper, N. Hansen, T.A. Cool, P.R. Westmoreland, Proc. Combust. Inst. 32 (2009) 1269–1276.
[70] Z.Y. Tian, Y.Y. Li, T.C. Zhang, A.G. Zhu, F. Qi, J. Phys. Chem. A 112 (2008) 13549–13555.
[71] Z.Y. Tian, Y.Y. Li, T.C. Zhang, A.G. Zhu, Z.F. Cui, F. Qi, Combust. Flame 151 (2007) 347–365.
[72] M. Hori, N. Matsunaga, N. Marinov, W. Pitz, C. Westbrook, Proc. Combust. Inst. 27 (1998) 389–396.
[73] J.C. Biordi, Prog. Energy Combust. Sci. 3 (1977) 151–173.
[74] U. Struckmeier, P. Oβwald, T. Kasper, L. Böhling, M. Heusing, M. Köhler, A. Brockhinke, K. Kohse-Höinghaus, Z. Phys. Chem. 223 (2009) 503–537.
[75] J.C. Biordi, C.P. Lazzara, J.F. Papp, Combust. Flame 23 (1974) 73–82.
[76] O.I. Smith, D.W. Chandler, Combust. Flame 63 (1986) 19–29.
[77] D. Stepowski, D. Puechberty, M.J. Cottereau, Proc. Combust. Inst. 18 (1981) 1567–1573.
[78] G.P. Smith, D.M. Golden, M. Frenklach, N.W. Moriarty, B. Eiteneer, M.C. Goldenberg, T. Bowman, R. Hanson, S. Song, W.C. Gardiner Jr., V. Lissianski, Z. Qin. Available from: <http://www.me.berkeley.edu/grimech>.
[79] C. Morley, Combust. Flame 27 (1976) 189–204.
[80] B.S. Haynes, Combust. Flame 28 (1977) 81–91.
[81] A.C. Baldwin, D.M. Golden, Chem. Phys. Lett. 55 (1978) 350–352.
[82] M. Frenklach, H. Wang, C.T. Bowman, R.K. Hanson, G.P. Smith, D.M. Golden, W.C. Gardiner Jr., V. Lissianski, GRI-Mech version 2.1, released June 1995, CHEMKIN-II format. Available from: <http://www.me.berkeley.edu/grimech>.
[83] C. Wilson, G.G. Balint-Kurti, J. Phys. Chem. A 102 (1998) 1625–1631.
[84] S. Bauerle, M. Klatt, H.G. Wagner, Ber. Bunsenges. Phys. Chem. 99 (1995) 870–879.
[85] A.W. Jasper, S.J. Klippenstein, L.B. Harding, J. Phys. Chem. A 111 (2007) 8689–8707.
[86] M.A. Blitz, K.W. McKee, M.J. Pilling, P.W. Seakins, Chem. Phys. Lett. 372 (2003) 295–299.
[87] P. Glarborg, L.L.B. Bentzen, Energy Fuels 22 (2008) 291–296.
[88] S.H. Song, D.M. Golden, R.K. Hanson, J.P. Senosaian, C.B. Musgrave, G. Friedrichs, Int. J. Chem. Kinet. 35 (2003) 304–309.
[89] K.H. Becker, B. Engelhardt, H. Geiger, R. Kurtenbach, P. Wiesen, Chem. Phys. Lett. (1993) 135–140.
[90] R.Q. Zhang, K.L. Han, R.S. Zhu, C.S. Lee, S.T. Lee, Chem. Phys. Lett. 321 (2000) 101–105.
[91] S.A. Carl, J.N. Crowley, J. Chem. Phys. A 102 (1998) 8130–8142.